VOLUME 2, 2019
DOI: 10.31058/j.ap.2019.21001

Determination of the Crystallite Size & Micro- Strain by Novel Method from XRD Profile

Emad A Badawi [1*], M A Abdel-Rahman[1], A Mostafa[1], M. Abdel-Rahman[1]

[1] Physics Department, Faculty of Science, Minia University, Egypt

Email Address

emad.badawi@mu.edu.eg (Emad A Badawi), m_abdelrahman@mu.edu.eg (M Abdel-Rahman)
*Correspondence: emad.badawi@mu.edu.eg

Received: 15 November 2018**; Accepted:** 31 December 2018**; Published:** 21 January 2019

Abstract:

In the present work, an approximation novel method was used to determine both the crystallite size and micro-strain from XRD profile for deformed and non-deformed 3004 Al alloy by determining the total physical broadening, the crystallite size broadening and the strain broadening. Aluminum and its alloys are widely used in aircraft automotive and in construction industries because of their desirable physical properties. The estimated crystallite size and micro-strain obtained via this approximation method were in a good agreement with the full width at half maximum (FWHM) and the strain broadening at each peak (111), (200), (220), (311), (222) at the corresponding Bragg angles. The variation of strain broadening, defect density and stored dislocation energy with thickness reduction seems to be an exponential growth, according to the increasing of the dislocation density as predicted theoretically.

Keywords:

XRD Profile, Estimated Crystallite Size, Full Width at Half Maximum, Micro-Strain, Stored Dislocation Energy, Strain Broadening, Defect Density

1. Introduction

The non-heat-treatable 3004 wrought Al-alloy is one of aluminum-manganese series (3xxx) which covering a large area in assorted applications for their conspicuous properties for being light in weight, having good electrical and mechanical properties, etc. precipitation hardening by strengthening has no effect on these alloys which are hardened by cold work (plastic deformation due to compression). Plastic deformation is a perpetual shape change that is irreversible even after taking off the applied load. It can be considered as a dominant phenomenon when the applied load on metals or alloys exceeds the demand dislocation energy movement. A “dislocation” as a line formed defect by the permanent deformation is made in the interior crystalline solid [1-2]. 3004 aluminum alloys are obeying to different investigations because of the new ways for fabrication of these alloys and ways of enhancing their properties.

The control and adjusting of microstructural parameters during the permanent deformation makes widely utilization for these alloys. Nowadays, the demand for 3004 Al-alloys have increased than other materials. Cold compression is commonly used as the perpetual deformation processing of these alloys. The factors that control the microstructure parameters during plastic deformation are Crystallite size, micro-strain and dislocation density. Both domain size and crystal morphology has a vital effect in various applications of this alloy, which enable the manufacturers to focus on the fabrication techniques and sort of modification done. There are different commercial techniques to study the microstructure of materials either in powder or in bulk state such as the scanning electron microscope (SEM), TEM and XRD. The used method in our work is XRD which was used to make analysis for the obtained diffracted lines from XRD pattern. To determine the defect or microstructure variations in a given XRD pattern for the investigated specimens, two well-known methods were used in this research, Scherer and its modified Williamson–Hall method [3-4].

X-Ray diffraction (XRD) is a nondestructive and vital quantitative method used in material science to study the internal structures of powder or bulk materials [4]. The XRD method is used to better analyze the presence of deformation, micro-deformation and domain size.

XRD results is generally recognized for its accurate evaluation of crystallographic structure parameters such as micro-strain, crystallite size and dislocation density, so it is suitable for technical applications [5]. Information about phase compositions, crystallographic preferred orientations and crystallographic defect concentrations is given by XRD data analysis [6]. One of the reliable features of XRD data is the peak or line broadening which can be detected because of the variations in the crystallographic lattice structure of the tested samples. The result of small crystallite size in the growth direction of the strains, stacking faults, dislocations and point defects is caused by the peak broadening. The domain size broadening is made by the finite size components' diffracting incoherently with respect to one another but the strain broadening is caused by the non-uniform displacements of the atoms with respect to their reference-positions in the lattice.

Because of the limited size of the crystal, there is an ejection from the ideal arrangement of atoms producing real crystals which leads to broadening of the X-ray diffraction lines [7]. The diffracted lines in the XRD pattern can be directly quantified. It should take in our consideration that the crystallographic broadening (observed broadening) is a result of factors viz. instrumental effects, crystallite size and lattice strain. The physical broadening is determined by measuring the angular width "β", in radians, at intensity equal to half the maximum intensity (FWHM). Subtracting the instrumental effect from the obtained peak broadening, two main properties; crystallite size and lattice strain are extracted from peak width analysis [8]. Crystallite size and lattice strain affect the Bragg peak by increasing the peak width and intensity and shift the 2(θ) peak position accordingly. The crystallite size varies as 1/cos (θ) and stain varies as tan (θ) from the peak width [4].

In this work, a novel method was applied. This method would be useful to determine both crystallite size and micro-strain by XRD broadening analysis since it is reliable, convenient and less time-consuming procedure. The novel method was briefly described in determining the broadening parameters of crystallite size and microstrain of aluminum alloys. Comparisons of crystallite size, microstrain and

dislocation density using Scherrer formula and Williamson–Hall method were highlighted. The validity of the novel method for the broadening parameters was discussed.

2. Preparation of Tested Samples and the Used Technique

In this work, firstly, the required specimens of 3004 Al-alloy which has a chemical composition as shown in Table 1 were cut with needed sizes and dimensions of (12 x 12 x 3) mm^3. This process was done by using an electrical cutter; secondly, grinding the surface of the specimens with silica carbide grinding papers of size 120, 220, 300, 600, 1000 and 1200 grit to produce a smooth finish on flat surfaces. This step enables us to reach a fine flat surface but soft enough. Thirdly, polishing of the specimens was done to create a smooth and shiny surface by rubbing it or using a chemical action, leaving a surface with a significant specular reflection. Fourthly, these investigated samples annealed at 450℃ in a furnace without vacuum to avoid residual or injected stresses and then cleaned with needed solution and dried. Finally the samples were deformed at levels from 0.00% to 33% thickness reduction (at room temperature) to be equipped for work.

X-ray source at 40 kV and 35 mA was used for continuous scanning with a slow scanning rate (1^o /min) and a small time constant (1sec) using a JEOL X-ray diffractometer (XRD) (Model JSDX-60PA) prepared with a Cuk α-radiation (λ= 0.145184 nm). A range of 2θ (from 30^o to 90^o) was scanned so that the needed diffraction lines for phase identification could be obtained. XRD was concerned for the phase identification and crystallographic preferred orientation [9].

Table 1. *The chemical composition of 3004 Al-alloy.*

Element	Si	Fe	Cu	Mn	Mg	Zn	others	Al
Wt %	0.3	0.7	0.25	1.0-1.5	0.8-1.3	0.25	0.15	reminder

3. Results and Discussion

3.1. Estimation of the Crystallite Size Broadening (FWHM) and the Strain Broadening at Each Plane

X-ray diffraction (XRD) pattern was recorded for the non-deformed and deformed alloys under investigations at different states of thickness reduction as shown in Figure 1. In order to calculate the FWHM due to crystallite size and strain broadening of 3004 wrought aluminum alloys, XRD measurements were done for all samples under investigation. Intensity as a function of the diffraction angle 2(θ) of the tested samples were introduced in Figure 1. For real polycrystalline materials, the intensity profile tends to be broader because of two main imperfections: Scattering from small coherent domains (Scherrer, 1918), and internal micro-strain associated with variations in the d-spacing of the scattering crystals (Stokes and Wilson, 1944) [10,11].

The experimental intensity profile (observed intensity profile) can be regarded as a convolution of two profiles. The first is from a real polycrystalline sample and the latter is due to non-ideal experimental conditions. The latter is known as the instrumental profile and its broadening arises from factors such as, axial divergence, flatness, transparency and surface roughness of the sample (Wilson, 1962)[11].

In order to extract the real crystal profile from the total physical broadening, it is necessary to deconvolute the instrumental broadening from the experimental profile. The full width at half maximum (FWHM) is used as a measure of the total broadening in this work. By performing line profile fitting to the experimental diffraction results, the FWHM is evaluated for every diffraction peak. Fitting the best polynomials (in this case second order) to the sample's and to a reference samples FWHMs as a function of (θ) gives a continuous representation of the experimental $\beta_e(\theta)$ and instrumental $\beta_i(\theta)$ broadening respectively. The de-convolution of $\beta_i(\theta)$ from $\beta_e(\theta)$, i.e., the calculation of the broadening coming from the real crystals $\beta(\theta)$, can be obtained by one of the following methods [11]:

$$\beta_e(\theta)^2 = \beta_o(\theta)^2 - \beta_i(\theta)^2 \quad (1)$$

$$\beta_e(\theta) = \beta_o(\theta) - \beta_i(\theta) \quad (2)$$

Equations (1) and (2) assume Gaussian and Lorentzian forms of diffraction peaks, respectively. In this work Gaussian fitting was used and Equations. (1), (2) can be written as follows [9]:

$$\beta_e^2 = \beta_o^2 - \beta_i^2 \quad (3)$$

$$\beta_e = \beta_o - \beta_i \quad (4)$$

$$\beta_e = \beta_c + \beta_s \quad (5)$$

Where

(β_o) is the observed or total physical broadening (FWHM) which is equal to the sum of the experimental and instrumental broadening.

(β_i) is the instrumental broadening (FWHM) which is due to non-ideal experimental conditions and is approximately equal to 0.048^o or 8.465×10^{-4}Radian or (Rad).

(β_e) is the experimental broadening (FWHM) which can be regarded as a convolution of two profiles, i.e., the sum of the broadening due to crystallite size (β_c) and lattice strain (β_s) as shown in Figure 2, Figure 3.

The domain size broadening and micro-strain broadening as the reason of crystallographic dislocations can be obtained according to Scherrer and Williamson-Hall methods from the wealth XRD information as follow [12]:

$$\beta_c = \frac{k\lambda}{L_c \cos(\theta)} \quad (6)$$

$$\beta_s = 4\,\varepsilon \tan(\theta) \quad (7)$$

$$\beta_e = \beta_{hkl} = \frac{k\lambda}{L_c \cos(\theta)} + \eta\, tan(\theta) \quad (8)$$

$$\eta = 4\,\varepsilon \quad (9)$$

Where $k = 0.94$ is the Scherrer constant, L_c is the Scherrer crystallite size, (θ) is the Braggs angle, (η) is the external strain of the tested sample and (ε) is the lattice strain and often known as microstrain [13].

3.2. Derivation of a Novel Method for Broadening Calculations

From Figure 2, Figure 3, the black curve is the experimental (pure) peak area (β_e) which can be considered as the mixture of the broadening due to crystallite size (β_c) and microstrain (β_s) according to the Williamson-Hall Method. The percentage of (β_c) in the mixture, is equal to the ratio (R_c) and the percentage of (β_s) in the same mixture is equal to the ratio (R_s) as follows:

$$(R_c) = \frac{\beta_c}{\beta_e} \tag{10}$$

$$(R_s) = \frac{\beta_s}{\beta_e} \tag{11}$$

If we add

$$(R_c) + (R_s) = \frac{\beta_c}{\beta_e} + \frac{\beta_s}{\beta_e} = \frac{\beta_c + \beta_s}{\beta_e} = 100\ \%\ \text{ i.e. } \beta_e = \beta_c + \beta_s \tag{12}$$

Some facts should take in our considerations:

According to according to Williamson-Hall Method, the total crystallite broadening ($\beta_{hkl} = \beta_e$) is equivalent to the broadening due to the crystallite size only (β_c) except small crystallite value which known as the crystallite strain (β_s) [12].

From the software origin program, after, we make fitting for the experimental data, we find that the experimental peak area ($\beta_{hkl} = \beta_e$) is equivalent to the theoretical fitting (β_f) except small observed shift (β_{sh}) [14].

According to the strain law: Strain = Change in size/Original size [15]

From the above facts we can conclude that:

The broadening due to the crystallite size only (β_c) is equivalent to theoretical fitting (β_f) and the observed shift in broadening (β_{sh}) is equivalent to (β_s), so the broadening due to microstrain only (%) is given by:

$$\beta_s = \frac{\beta_e - \beta_c}{\beta_e} \tag{13}$$

And also the broadening due to the crystallite size only(%) is given by:

$$\beta_c = \frac{\beta_e - \beta_s}{\beta_e} \tag{14}$$

Now, we will prove the correctness of equations (13, 14) if we determine (R_c) and (R_s). By multiply both sides of equation (13) we obtain:

$$\beta_s \beta_e = \beta_e - \beta_c \tag{15}$$

$$\beta_s \beta_e + \beta_c = \beta_e$$

$$\beta_c = \beta_e - \beta_s \beta_e$$

$$\beta_c = \beta_e (1 - \beta_s)$$

$$\frac{\beta_c}{\beta_e} = (1 - \beta_s) \tag{16}$$

From equation (12), equation (16) can be written as:

$$\frac{\beta_c}{\beta_e} = (\beta_e - \beta_s \tag{17}$$

(17) is the same as equation (10), so this proof is correct. This method is reliable, convenient and less time-consuming procedure which enables us to use any one of the well-known methods e.g Scherrer, Williamson-Hall method or the Integral Breadth method in determining the microstructural parameters by determining the total physical broadening, crystallite size broadening and strain broadening.

Figure 1 indicates the diffraction pattern at each plane for 3004 Al-alloy. According to the above equation(6), the full width at half maximum due to the crystallite size only given at each plane is shown in Figure 4, the total crystallite broadening (total FWHM) is shown in Figure 5 and their average comparison is shown in Figure 6.

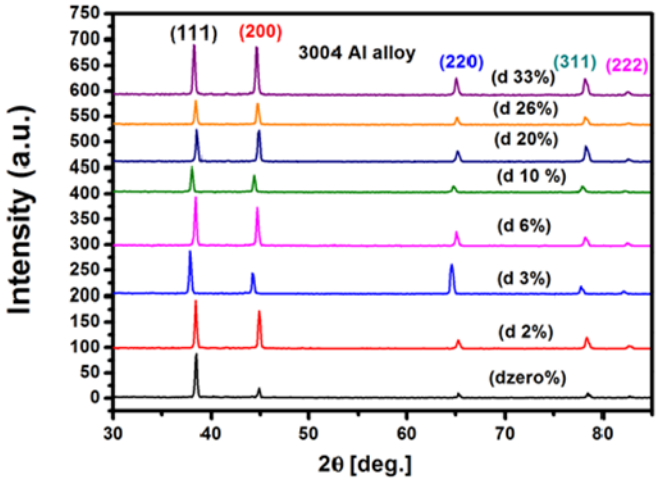

Figure 1. *XRD pattern of 3004 Al-alloy at different deformations for intensity versus 2(θ). Note that a.u refers to arbitrary unit, deg. refers to degree and (d) is the abbreviation of deformation.*

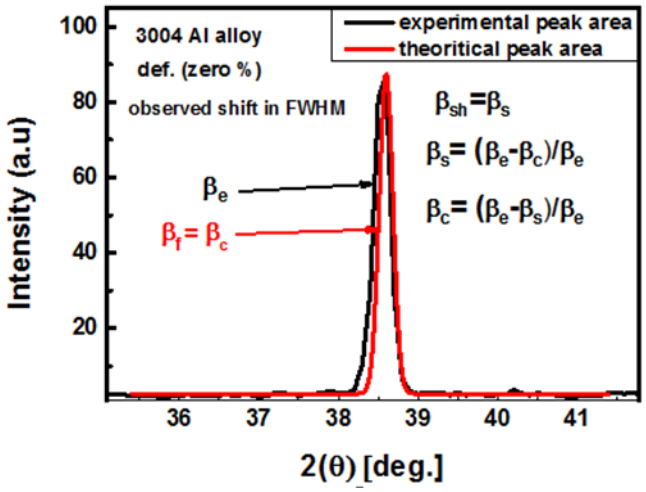

Figure 2. *Intensity versus 2(θ) for the peak (111) at (zero %) deformation for 3004 Al -alloy. Note that, (def.) is the abbreviation of deformation.*

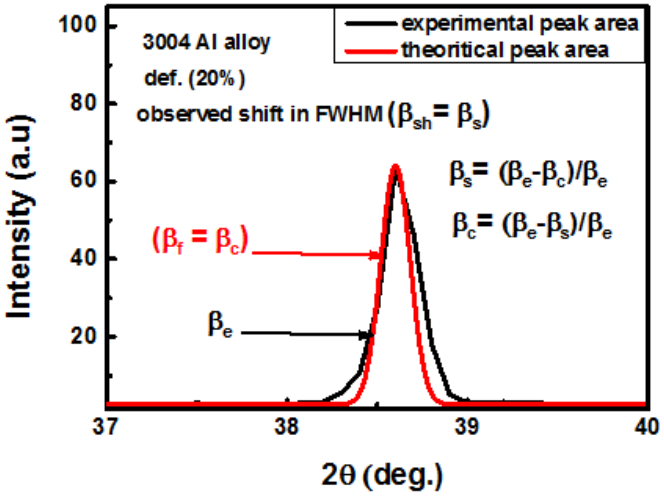

Figure 3. *Intensity versus 2(θ) for the peak (111) at (20 %) deformation for 3004 Al- alloy.*

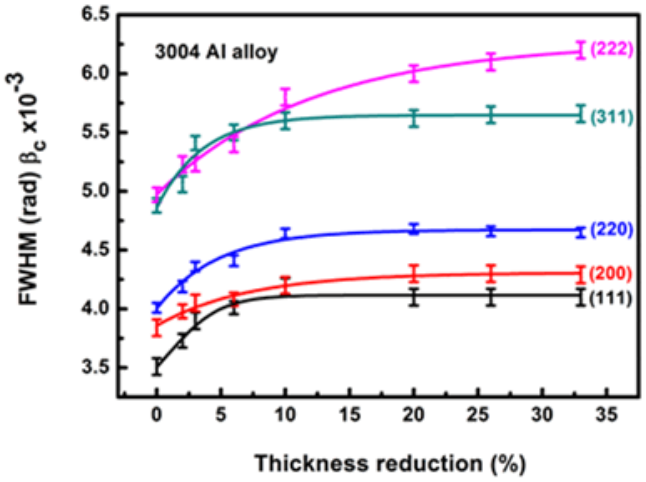

Figure 4. *The (FWHM) due to crystallite size only (β_c) versus thickness reduction at the different 5 planes for 3004 Al- alloy.*

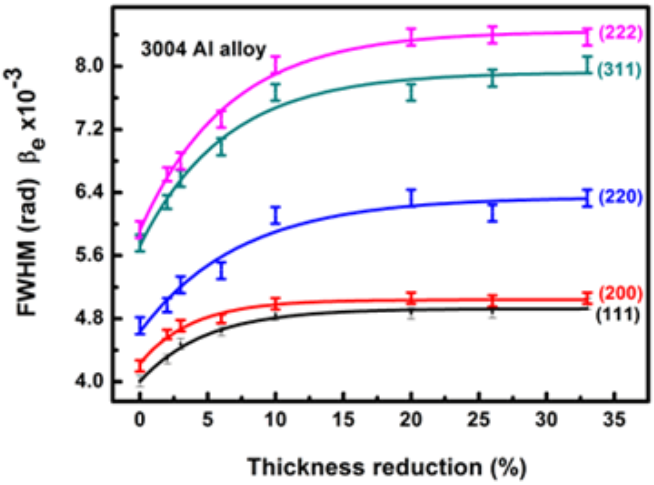

Figure 5. *The total FWHM (β_e) versus thickness reduction at the different 5 planes for 3004 Al-alloy.*

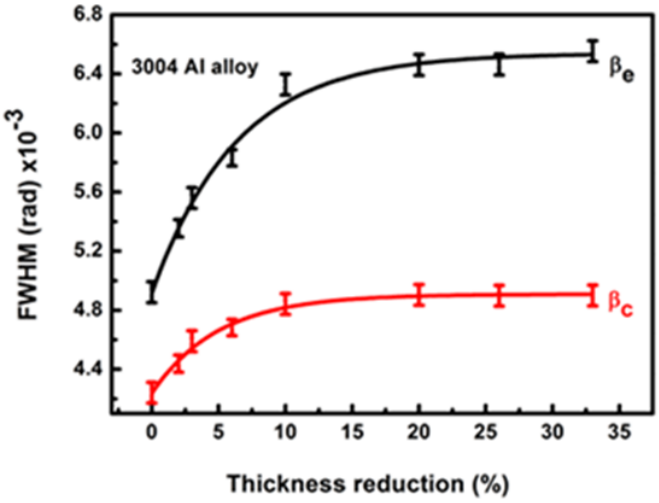

Figure 6. *The average FWHMs (β_e) and (β_c) versus thickness reduction for 3004 Al -alloy.*

Similarly, according to Wilson, the broadening due to lattice strain may be expressed as the strain broadening (β_s) of 3004 Al-alloy which can be calculated from

equation (13).The strain broadening (β_s) and its average of 3004 Al-alloy is increased exponentially with degree of thickness reduction for the investigated samples as shown in the given Figure 7, Figure 8) where the abbreviation of (D.U) refers to dimensionless unit.

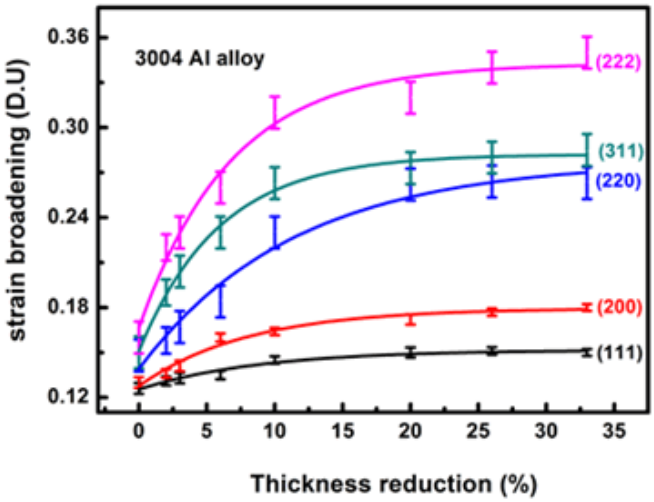

Figure 7. *The strain broadening versus thickness reduction at the different 5 planes for 3004 Al-alloy.*

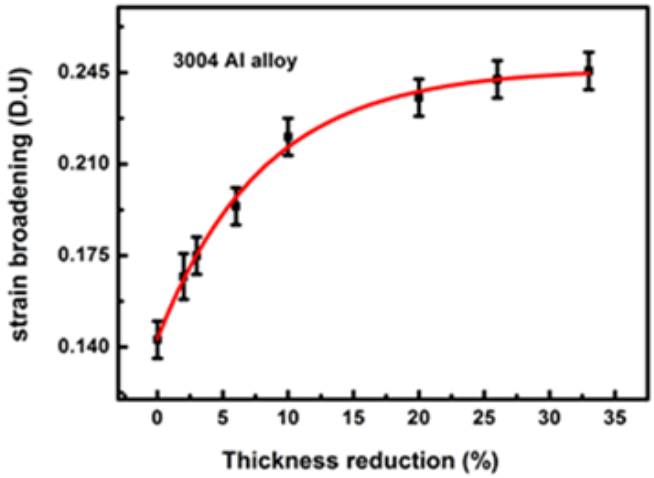

Figure 8. *The average strain broadening versus thickness reduction for 3004 Al-alloy.*

3.3. Estimation of Crystallite Size and Wilson Lattice Strain

For the domain size and micro-strain calculations, X-ray detection was made for all tested samples. Not only there is essential characteristics of the diffraction pattern are the same but also a sensitive change in the line intensity is detected. The diffraction peaks at [2θ = 38.7, 44.9, 65.3, 78.4 and 82.6] respectively, correspond to [(111), (200), (220), (311) and (222)] planes of face centered cubic aluminum as confirmed by JCPDS X-ray file data. However, in all states the intensities of (111) and (200) were extremely high in comparison with the other reflections, indicating that they are the preferential orientation of micro crystallites.

The Scherrer crystallite size (L_c), Williamson-Hall crystallite size (L_e) and their average as function of thickness reduction of 3004 Al-alloy at the different 5 peaks were calculated by using equations (6, 8). It was found that the mean domain size

decreases exponentially as a function of thickness reduction as shown in Figure 9, Figure 10, Figure 11).

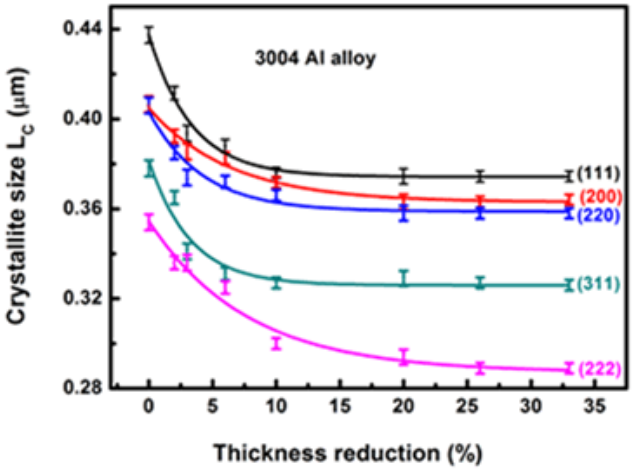

Figure 9. *The Scherrer crystallite size (L_c) versus thickness reduction at the different 5 planes for 3004 Al- alloy.*

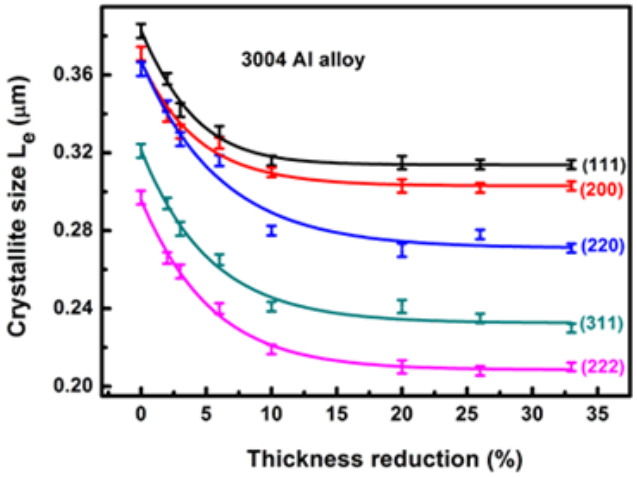

Figure 10. *The Williamson-Hall crystallite size (L_e) versus thickness reduction at the different 5 planes for 3004 Al- alloy.*

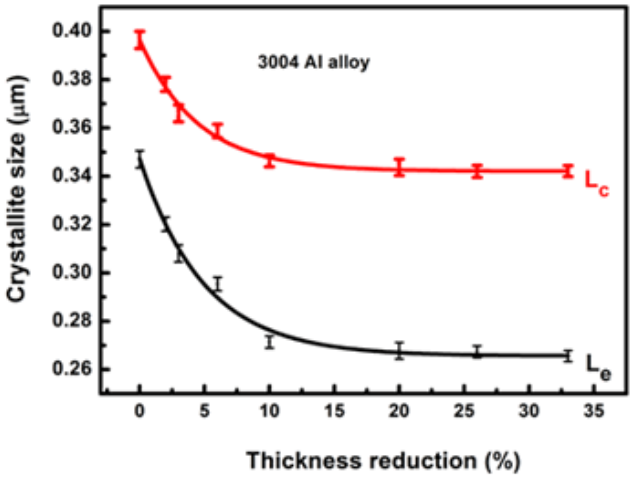

Figure 11. *The average crystallite size (L_c) and (L_e) respectively versus thickness reduction measured for 3004 Al-alloy.*

On the other hand, micro-strain in a material causes variation in shapes and positions for the diffracted lines [16]. The micro-strain can give information about its effect on the crystallites for being the same in all ways or not, depending on the observed lines from being sharp or broadened. In general cases, there is a distribution of strains in all tested samples which therefore makes broadening in an angle of the diffraction lines, and the lines at higher Bragg angles are broadened more [17].

The same phenomenon is applied when the chemical composition of a material is inhomogeneous; the crystallographic atomic separation depends on chemical composition-diffraction peaks which are broadened. The micro-strain of 3004 Al -alloy was found to be increased exponentially as a changing of thickness reduction as shown in the given Figure 12, Figure 13) [11].

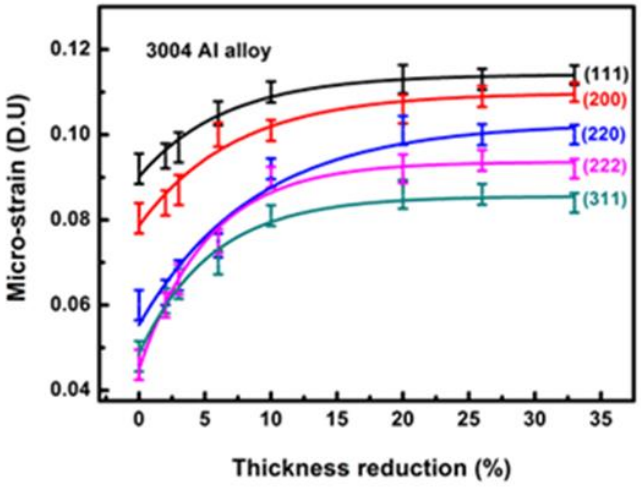

Figure 12. *The micro-strain versus thickness reduction at the different 5 planes for 3004 Al -alloy.*

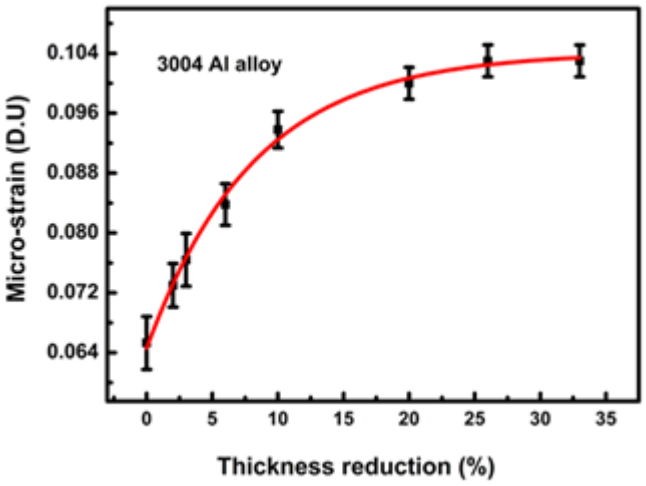

Figure 13. *The average micro-strain versus thickness reduction for 3004 Al -alloy.*

From equation (8), according to the Williamson-Hall method [18], we can determine the small portion contributions to the broadening results from reflections by using the following equation which can be expressed as:

$$\beta_e \cos\theta = \beta_{hkl} \cos\theta = \frac{k\lambda}{L_c} + \eta \sin\theta \qquad (18)$$

Williamson-Hall plot for different degree of deformation of the investigated samples and a linear fit of the scattered features was taken into our calculations as

shown in Figure 14. From this linearity, The Scherrer crystallite size (L_c), was estimated from the y-intercept, and the external strain, from the slope of the fit [19]. It was found that the value of the slope=0.03 i.e $\eta = 0.03$, and the value of the intercept is equal to 0.128 but $\eta = 4\,\varepsilon$ i.e $\varepsilon = 0.12$ (%).

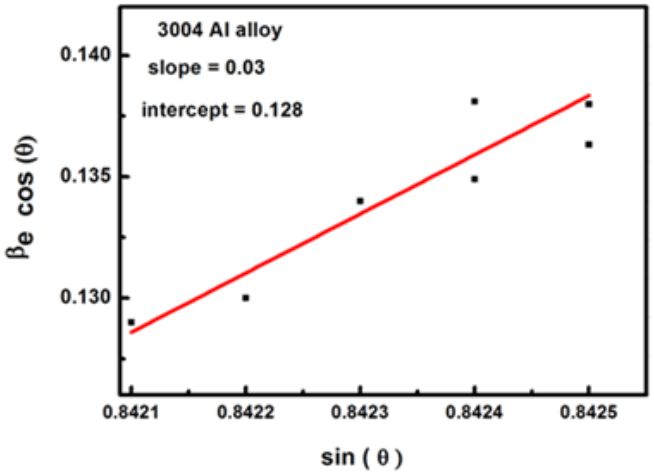

Figure 14. *$\beta_e\, cos(\theta)$ versus sin (θ) for 3004 Al alloy.*

During deformation of metals or alloys dislocations are stored as energy which plays a vital role in most metallurgical phenomena such as strain hardening, damage, creep, fatigue, a thermal phase transformations, recrystallization and strain induced grain boundary migration. The stored dislocations have mechanical strong effect on materials such as strength and ductility during annealing and transformation of deformed microstructures. The average dislocation density has a relation with different phenomenon such as creep rate, strengthening and recovery. Dislocation density(ρ) is widely calculated by this relation [21].

$$< \varepsilon^2 >^{1/2} = \frac{\rho\, L\, b}{3\sqrt{2\pi}} \tag{19}$$

In a material science, the micro strain is the root mean square of the variations in the lattice parameters across the individual crystallites, usually across microscopic distances$< \varepsilon^2 >^{\frac{1}{2}}$, (ρ) is the dislocation density, L is the mean crystallite size, b = 0.286 nm is the burger vector of FCC material 3004 Al-alloy. The Scherrer dislocation density (ρ_c) and Williamson-Hall dislocation density (ρ_e), were changed exponentially with thickness reduction as show in the given Figure 15.

They related to the defect density ρ—(cm-3) by the given relation as follows [22], while their defect densities were shown in Figure 16.

$$\rho^{-}(\mathrm{cm}^{-3}) = \frac{\rho(cm^{-2})}{b} \tag{20}$$

In most cases, the flow stress as a changing in the resolved shear stress (τ) relates to the square root of dislocation density as follows [21]:

$$\tau = \tau_0 + \alpha\, Gb\sqrt{\rho} \tag{21}$$

Where τ_0 is the stress of friction, $\alpha = 0.5$ is a constant, G=26 GPa is the bulk modulus of Al, and b is Burgers vector. In terms of tensile stress, by taking the friction stress equal to zero and $\sigma = M\,\tau$, the flow stress (σ) is calculated for the tested alloys by the relationship [21]:

$$\sigma = M\alpha\, Gb\sqrt{\rho} \tag{22}$$

Where (M) is the average Taylor factor, then the above relation is given by [21],

$$\tau = \alpha\, Gb\sqrt{\rho} \tag{23}$$

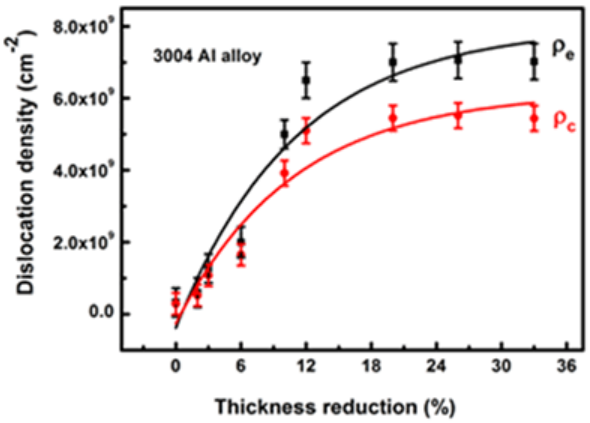

Figure 15. *The average dislocation density (ρ_e) and (ρ_c) versus thickness reduction for 3004 A-l alloy.*

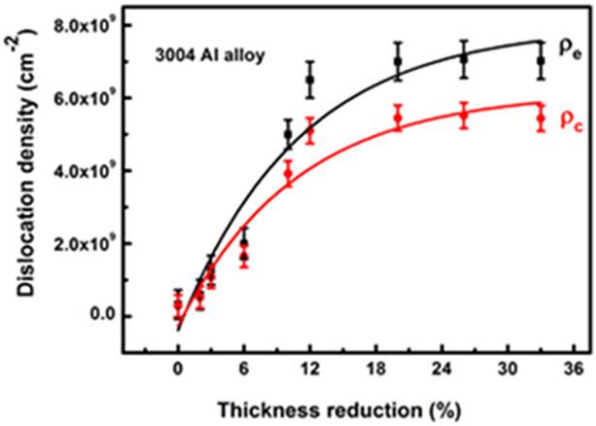

Figure 16. *The average defect density (ρ_e^-) and (ρ_c^-) versus thickness reduction for 3004 Al- alloy.*

The Scherrer flow stress(τ_c) and Williamson-Hall flow stress(τ_e), were changed exponentially with thickness reduction as show in the given Figure 17.

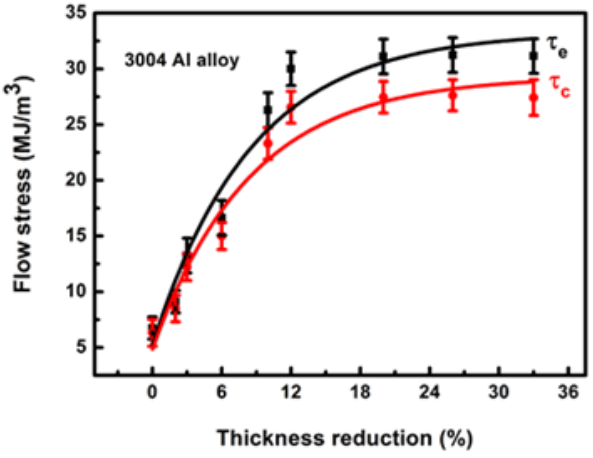

Figure 17. *The average flow stress (τ_e) and (τ_c) versus thickness reduction for 3004 Al -alloy.*

Small internal energy of the investigated samples was formed because of the cold deformation in the region of plasticity. This increment in the stored energy is related to the defects generated during deformation. In deformed samples the dislocation density is a function of the domain size which was higher in fine-grained than in coarse-grained aggregates at the same strain.

On this basis, the stored energy should be a sensitive function of the particle size, especially at low strains. Both the stored energy and the manner in which the stored energy is released rely on the domain size. The dislocation density ρ has useful relation with the dislocation stored energy (E) as [1] as shown in Figure 18.

$$E = \alpha G b^2 \rho \quad (24)$$

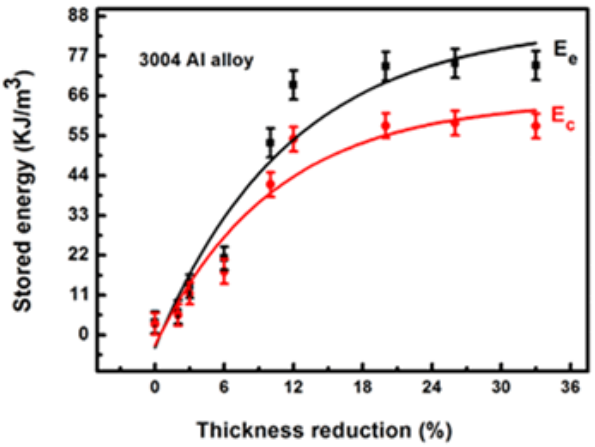

Figure 18. *The average stored energy (E_e) and (E_c) versus thickness reduction for the 3004 Al - alloy.*

The Scherrer stored energy (E_c) and Williamson-Hall stored energy (E_e), were changed exponentially with thickness reduction as shown in Figure 18.

4. Conclusions

According to the results and discussion the following items we can conclude:

I. An important method was successfully applied to calculate the FWHM and the strain broadening which used to calculate the crystallite size and micro-strain by the line broadening analysis of the XRD peaks of the investigated 3004 Al alloy.

II. The FWHM and the strain broadening were calculated at the different 5 peaks at the different Bragg angles and it was observed that both of them increases exponentially as a function of thickness reduction.

III. The micro-structural parameters, e.g. crystallite size and micro-strain were calculated at the different 5 peaks and they have good correlation with FWHM where the crystallite size decreases exponentially with FWHM but micro-strain increases exponentially with FWHM.

IV. The flow stress increases exponentially with thickness reduction.

V. The dislocation density, defect density and stored dislocation energy were evaluated which they presented an exponential increase as a function of thickness reduction for the investigated sample.

Conflicts of Interest

The author declares that there is no conflict of interest regarding the publication of this article.

References

[1] Abdel-Rahman, M. Determination of the Positron Parameters and the Stored Dislocation Energy of Plastically Deformed Wrought 3004 Al-Alloy. *Int. J. New. Hor. Phys.* 2017, 4(2), 43-47.

[2] Sharma, S. R.; Ma, Z. Y.; Mishra, R. S. Effect of friction stir processing on fatigue behavior of A356 alloy. *Scripta Materialia*, 2004, 51(3), 237-241.

[3] Bindu, P., Thomas, S. Estimation of lattice strain in ZnO nanoparticles: X-ray peak profile analysis. *Journal of Theoretical and Applied Physics*, 2014, 8(4), 123-134.

[4] Bushroa, A. R.; Rahbari, R. G.; Masjuki, H. H.; Muhamad, M. R. Approximation of crystallite size and microstrain via XRD line broadening analysis in TiSiN thin films. *Vacuum*, 2012, 86(8), 1107-1112.

[5] Kasatkin, I.; Kurr, P.; Kniep, B.; Trunschke, A.; Schlögl, R. Role of lattice strain and defects in copper particles on the activity of Cu/ZnO/Al2O3 catalysts for methanol synthesis. Angewandte Chemie International Edition, 2007, 46(38), 7324-7327.

[6] Klug, H. P.; Alexander, L. E. X-ray diffraction procedures: for polycrystalline and amorphous materials. X-Ray Diffraction Procedures: For Polycrystalline and Amorphous Materials, 2nd Edition, by Harold P. Klug, Leroy E. Alexander, pp. 992. ISBN 0-471-49369-4. *Wiley-VCH*, 1974., 992.

[7] Ribárik, G.; Gubicza, J.; Ungár, T. Correlation between strength and microstructure of ball-milled Al–Mg alloys determined by X-ray diffraction. *Materials science and engineering: A*, 2004, 387, 343-347.

[8] Ortiz, A. L.; Shaw, L. X-ray diffraction analysis of a severely plastically deformed aluminum alloy. *Acta Materialia*, 2004, 52(8), 2185-2197.

[9] Mishra, S. K.; Roy, H.; Lohar, A. K.; Samanta, S. K.; Tiwari, S.; Dutta, K. (). A comparative assessment of crystallite size and lattice strain in differently cast A356 aluminium alloy. In IOP Conference Series: *Materials Science and Engineering*, 2015, 75(1), 012001.

[10] Chen, H.; Alpas, A. T. Wear of aluminium matrix composites reinforced with nickel-coated carbon fibres. *Wear*, 1996, 192(1-2), 186-198.

[11] Kimmel, G.; Dayan, D.; Frank, G. A.; Landau, A. X-ray diffraction (XRD) characterization of microstrain in some iron and uranium alloys (No. IA--1500), 1996.

[12] Kumar, S. S. V.; Venkateswara, R. K. X-ray peak broadening analysis and optical studies of ZnO nanoparticles derived by surfactant assisted combustion synthesis. *Journal of Nano-and Electronic Physics*, 2013, 5(2), 02026-1.

[13] Al-Jubory; A. A. Study of the effect of copper doping on the structural and optical properties of Cd0. 7Zn0. 3S nanocrystalline thin films prepared by

chemical bath deposition. *International Journal of Science and Technology*, 2012, 2(10).

[14] Seifert, E. OriginPro 9.1: Scientific Data Analysis and Graphing Software Software Review, 2014.

[15] Rehani, B. R.; Joshi, P. B.; Lad, K. N.; Pratap, A. Crystallite size estimation of elemental and composite silver nano-powders using XRD principles, 2006.

[16] Prabhu, Y. T.; Rao, K. V.; Kumar, V. S. S.; Kumari, B. S. X-ray analysis by Williamson-Hall and size-strain plot methods of ZnO nanoparticles with fuel variation. *World Journal of Nano Science and Engineering*, 2014, 4(01), 21.

[17] Guinebretière, R. X-ray diffraction by polycrystalline materials. John Wiley & Sons, 2013.

[18] Kumar, L.; Kumar, P.; Narayan, A.; Kar, M. Rietveld analysis of XRD patterns of different sizes of nanocrystalline cobalt ferrite. *International Nano Letters*, 2013, 3(1), 8.

[19] Mitra, P.; Mondal, S. Structural and morphological characterization of ZnO thin films synthesized by SILAR. *Progress in theoretical and applied physics*, 2013, 1, 17-31.

[20] Gutierrez-Urrutia, I.; Raabe, D. Dislocation density measurement by electron channeling contrast imaging in a scanning electron microscope. *Scripta Materialia*, 2012, 66(6), 343-346.

[21] Dini, G.; Ueji, R.; Najafizadeh, A.; Monir-Vaghefi, S. M. Flow stress analysis of TWIP steel via the XRD measurement of dislocation density. *Materials Science and Engineering: A*, 2010, 527(10-11), 2759-2763.

[22] Abdel-Rahman, M. A.; Kamel, N. A.; Abdel-Rahman, M.; Abo-Elsoud, M.; Lotfy, Y. A.; Badawi, E. A. Defect Densities Using the Positron Annihilation Doppler Broadening Technique in Wrought Alloys 3003 and 3005. In Defect and Diffusion Forum, Trans Tech Publications, 2006, 251, 79-88.